Cluster observations of electron holes in association with magnetotail reconnection and comparison to simulations

C. Cattell,[1] J. Dombeck,[1] J. Wygant,[1] J. F. Drake,[2] M. Swisdak,[2] M. L. Goldstein,[3] W. Keith,[3] A. Fazakerley,[4] M. André,[5] E. Lucek,[6] and A. Balogh[6]

Received 31 March 2004; revised 10 September 2004; accepted 3 November 2004; published 19 January 2005.

[1] Large-amplitude (up to ~50 mV/m) solitary waves, identified as electron holes, have been observed during waveform captures on two of the four Cluster satellites during several plasma sheet encounters that have been identified as the passage of a magnetotail reconnection *x* line. The electron holes were seen near the outer edge of the plasma sheet, within and on the edge of a density cavity, at distances on the order of a few ion inertial lengths from the center of the current sheet. The electron holes occur during intervals when there were narrow electron beams but not when the distributions were more isotropic or contained beams that were broad in pitch angle. The region containing the narrow beams (and therefore the electron holes) can extend over thousands of kilometers in the *x* and *y* directions, but is very narrow in the *z* direction. The association with electron beams and the density cavity and the location along the separatrices are consistent with simulations shown herein. The velocities and scale sizes of the electron holes are consistent with the predictions of *Drake et al.* [2003]. Particle simulations of magnetic reconnection reproduce the observed Cluster data only with the addition of a small (0.2 of the reversed field) ambient guide field. The results suggest that electron holes may sometimes be an intrinsic feature of magnetotail reconnection and that in such cases the traditional neglect of the guide field may not be justified. Very large amplitude lower hybrid waves (hundreds of millivolts per meter), as well as waves at frequencies up to the electron plasma frequency, were also observed during this interval.

Citation: Cattell, C., et al. (2005), Cluster observations of electron holes in association with magnetotail reconnection and comparison to simulations, *J. Geophys. Res.*, *110*, A01211, doi:10.1029/2004JA010519.

1. Introduction

[2] The importance of waves in the reconnection process has long been of interest, beginning with the recognition that in the Sweet-Parker model, the rate depended on the square root of the resistivity [*Parker*, 1957; *Sweet*, 1958], which was negligible in a collisionless plasma. Although *Petschek* [1964] showed that with the inclusion of slow mode shocks that widened the outflow region, the dependence was logarithmic, resistivity due to nonclassical collisions was still needed to break the frozen-in condition. Studies of wave data in the magnetopause and magnetotail, the regions within the Earth's magnetosphere where reconnection occurs, yielded varying conclusions about the importance of different wave modes and whether the observed wave amplitudes were adequate to produce enhanced electron-ion scattering sufficient to facilitate reconnection. A recent study of reconnection in a narrow (approximately c/ω_{pi}) Harris current sheet, utilizing a number of different simulation codes [*Birn et al.*, 2001], indicated that the rate of reconnection was the same as long as the Hall effect, which breaks the frozen-in condition for the ions, was included. Although these studies are sometimes interpreted to mean that microphysics is not important in reconnection, it is still necessary to understand the mechanism that decouples the electrons from the magnetic field, as well as heating and acceleration processes. Comparisons of three-dimensional (3-D) particle simulations of reconnection [*Drake et al.*, 2003] to Polar observations at the magnetopause [*Cattell et al.*, 2002a] have provided evidence that a nonlinear wave mode, electron holes, may play an important role in reconnection by scattering and energizing electrons. Observations of electron holes in association with reconnection have also been made by Wind in the magnetotail [*Farrell et al.*, 2002] and Geotail at the magnetopause [*Matsumoto et al.*, 2003].

[3] Because the Cluster satellites can measure simultaneously electric field waveforms at several locations within the current layer where reconnection is occurring, they provide the opportunity to study, in more detail, the role

[1]School of Physics and Astronomy, University of Minnesota–Twin Cities, Minneapolis, Minnesota, USA.
[2]Institute for Research in Electronics and Applied Physics, University of Maryland at College Park, College Park, Maryland, USA.
[3]NASA Goddard Space Flight Center, Greenbelt, Maryland, USA.
[4]Mullard Space Sciences Laboratory, University College London, Dorking, UK.
[5]Swedish Institute for Space Physics, Uppsala, Sweden.
[6]Space and Atmospheric Physics Group, Blackett Laboratory, Imperial College, London, UK.

0148-0227/05/2004JA010519$09.00

of electron holes and other wave modes in the dynamics of reconnection. In addition, the availability of electron pitch angle distributions that are accumulated in a short interval (0.125 s in the overlap energy band between the low- and high-energy detectors where the electron beams often occur) enables a one-to-one correlation of features in the distributions and the occurrence of electron holes. In this report, we describe observations obtained by Cluster on 1 October 2001 during a reconnection event in the magnetotail at ~18 R_E. This event has been the focus of several recent studies including *Runov et al.* [2003] and J. Wygant et al. (Cluster observations of an intense normal component of the electric field in the ion decoupling region at a thin reconnecting current sheet in the tail and its relation to non-adiabatic shock-like acceleration of ion beams, submitted to *Journal of Geophysical Research*, 2004, hereinafter referrred to as Wygant et al., submitted manuscript, 2004) and preliminary wave observations were described by *Cattell et al.* [2002b].

2. Data Set

[4] The electric field and spacecraft potential measurements utilized herein were made by the double-probe electric field instruments [*Gustafsson et al.*, 1988], which were designed to obtain bursts of high time resolution data in many different modes. Electric field data at frequencies from DC to kilohertz were obtained in the waveform captures described in this paper. These are the only measurements on Cluster (and in the magnetotail outside the 9 R_E apogee of the Polar satellite) that are obtained in an ''interferometric mode'' so that structure velocities can be directly measured, utilizing the single-probe voltages. The Cluster double-probe instrument makes a 2-D measurement of the electric field in the satellite spin plane (approximately the GSE *x*-*y* plane) with an 88 m tip-to-tip probe separation. The measurements of the spacecraft potential, which is indicative of density [*Pedersen*, 1995], were utilized to determine the orientation and propagation velocity of the plasma sheet boundary. The properties of the solitary waves were obtained from a cross-correlation analysis of the waveforms to obtain a time delay between opposing probes, yielding the solitary wave velocity and scale size [see *Dombeck et al.*, 2001]. The electric field along the spin axis ($\sim Z_{gse}$) is not measured. For this reason, wave amplitudes and the ratio of perpendicular to parallel components are likely to be underestimated. Because the magnetic field is primarily in the X_{gse} direction for these waveform captures, it is the perpendicular component of the field which is most affected. To produce the electric field in GSE and in magnetic field-aligned coordinates shown in Figures 1, 2, and 5, the assumption is made that the on-axis electric field is zero. In addition, to check possible amplitude ranges for the waves which are polarized primarily perpendicular to the magnetic field, the assumption that $\mathbf{E} \cdot \mathbf{B} = 0$ was utilized.

[5] The electron observations were obtained by the Plasma Electron and Current Experiment (PEACE) instrument [*Johnstone et al.*, 1997] in the SPINPAD mode which obtains a pitch angle scan in two energy bands (for this day, LEEA from ~1 eV to ~2 keV and HEEA from ~100 eV to ~30 keV) in two 0.125 s intervals in each spin period (4 s). HEEA and LEEA are looking in opposite directions, so that in the overlap energy range the complete pitch angle distribution can be obtained in 0.125 s. Electron density moments were also utilized. The magnetic field measurements are from the FGM instrument [*Balogh et al.*, 2001].

3. Observations of Electron Holes, Waves, and Electrons

[6] An overview of the interval of interest is shown in Figure 1, which plots the negative of the spacecraft potential (indicative of density), the three components of the magnetic field in GSM, and one component (E_{xgse}) of the ~10 s waveform capture electric field from all four Cluster satellites. Note that waves and solitary waves can not be identified in the waveform capture data on this scale; for this reason, two shorter (0.03 s) snapshots of the component of the electric field parallel to the magnetic field are shown to provide examples of solitary waves observed on C2 and C4. Cluster was located at ~18 R_E and 22.3 magnetic local time (MLT). See Figure 11 for a schematic of the spacecraft locations with respect to the inferred location of the *x* line. C3 was closest to the Earth and to the equatorial plane and to midnight. C4, the most tailward satellite, was ~2000 km tailward, C1 was farthest from the equatorial plane (~2000 km above C3). The black trace (C1) shows clearly that C1 tended to remain in the lobe or the plasma sheet boundary, while the other three satellites had multiple encounters with the current sheet. The spacecraft potential measurements were utilized to determine the orientation and speed of the current sheet during these events, as discussed in detail by Wygant et al. (submitted manuscript, 2004). Using this velocity to convert time to distance, it can be determined that the waveform captures on C2, C3, and C4 were obtained near the outer edge of the plasma sheet at distances of ~900–1800 km (approximately equal to a few c/ω_{pi}) from the center of the current sheet. There were nearly simultaneous waveform captures on C3 (from 0947:08.6 to 0947:19.2) and C4 (from 0947:09.4 to 0947:20), and the C2 and C1 waveform captures were ~1.5 and 4 min later, respectively. Comparison to *Runov et al.* [2003, Figure 1] shows that the captures on C3 and C4 were near the onset of tailward flow, the one on C2 was within the region of flow reversal, and the C1 capture was in the earthward flow after the *x* line moved tailward past the satellites. Note that there was also an *x* line passage just prior to this interval described herein.

[7] A variety of wave modes were observed during the four waveform captures, as revealed by the snapshots in the bottom two panels of Figure 1 and in Figure 2, which plots a 2 s snapshot of the GSE *y* component of the electric field obtained near the start of the waveform capture on each satellite. Note that the electron holes were seen at later times. All four satellites observed very large amplitude waves near the lower hybrid frequency (~5–10 Hz), polarized predominantly perpendicular to the magnetic field. The largest waves (up to ~250 mV/m) were seen by C3, and the smallest (up to ~100 mV/m) were seen by C1. The associated magnetic perturbations were ~1–5 nT. Waves with frequencies of ~20–30 Hz can also be identified on all satellites with amplitudes ranging from ~10 to ~25 mV/m. Waves in both these low-frequency bands persist (at lower amplitudes for the 5–10 Hz waves) throughout the ~10 s duration of the waveform captures. Note that the waves near

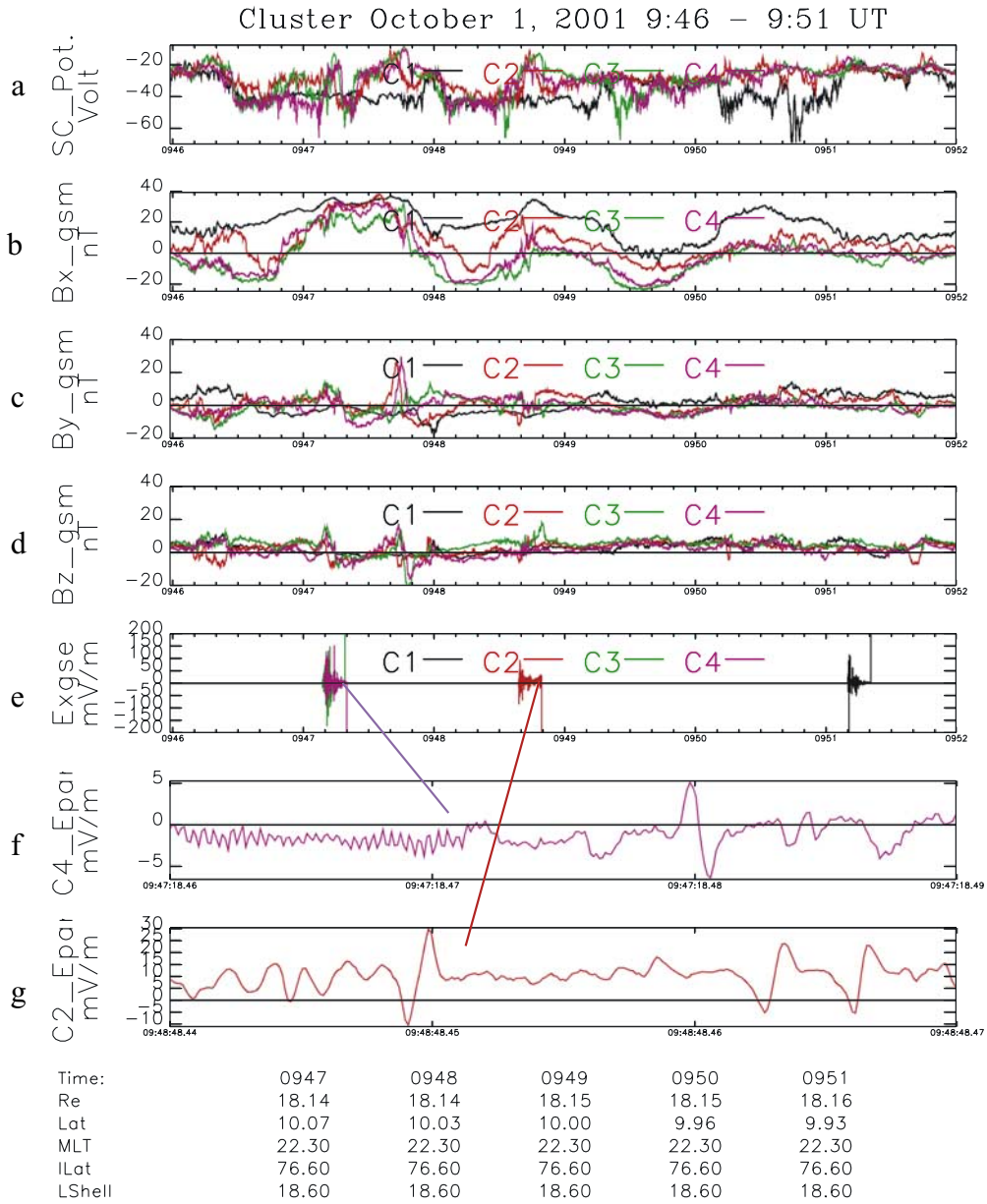

Figure 1. An overview of the plasma sheet crossings on 1 October 2001. (a) Negative of the spacecraft potential (SC_Pot), (b, c, and d) the three components of the magnetic field in GSM, (e) the *X*-GSE component of the electric field during the waveform captures (Exgse), and (f and g) an expanded view of the field-aligned component of the electric field for 0.03 s to show examples of the solitary waves on C4 (Figure 1f) and C2 (Figure 1g).

the lower hybrid frequency are also seen throughout the current sheet crossing, and these observations will be discussed in a forthcoming paper. With the exception of C1, all the satellites also observed higher-frequency waves (~1–5 kHz) near the electron plasma frequency.

[8] Solitary waves are only seen by C2 and C4; solitary waves were not identified on C1 or C3, either by eye or utilizing the automatic solitary wave program. The solitary waves on C2 (examples shown Figure 1g) occurred in association with waves near ~600 Hz (~0.1 f_{pe}), while those on C4 (example in Figure 1f) were associated with waves at ~2.6 kHz (~0.6 f_{pe}). These high-frequency waves were polarized primarily parallel to the magnetic field and are consistent with electron beam driven modes. The solitary waves had velocities of ~700 to >1500 km/s, with amplitudes up to 50 mV/m, and were positive potential structures. Many of the solitary wave signatures were asymmetric, consistent with a small net potential drop. Note that only a small fraction of the solitary waves could be timed; the rest were moving too fast or occurred when the angle between both pairs of the electric field probes and the magnetic field was too large for accurate timing. Therefore the currently available Cluster statistics on electron holes during reconnection events are not adequate to definitely conclude that the speed is always a fraction of the beam speed. For the solitary waves that were timed, $e\phi/kT_e$ was

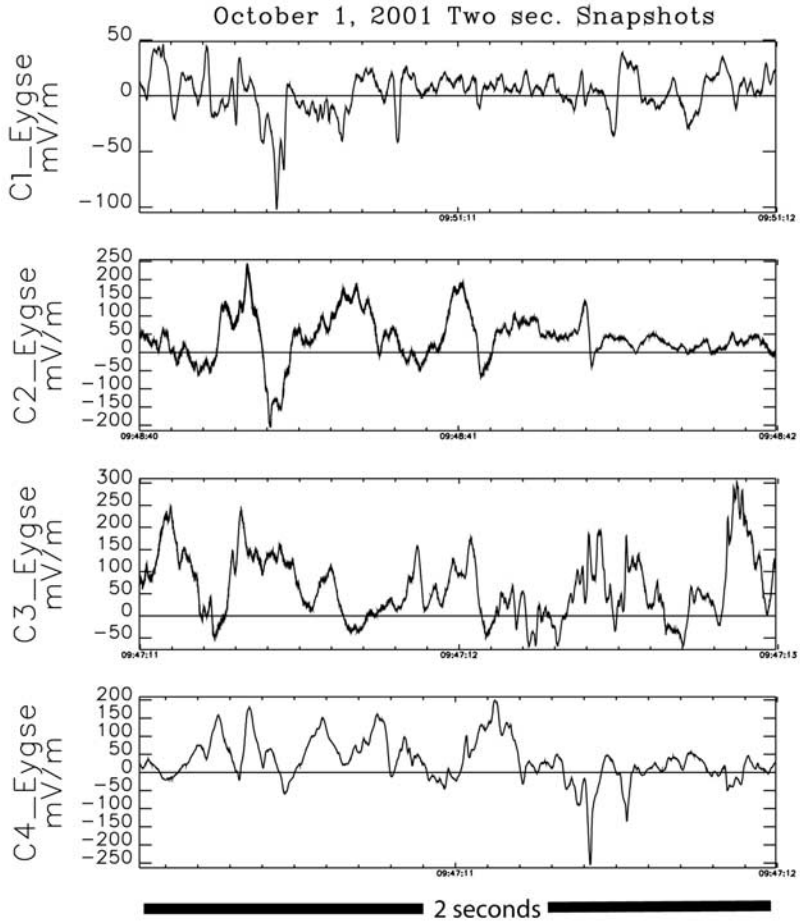

Figure 2. Two-second snapshots from the waveform captures on each of the Cluster satellites to show the types of low-frequency waves observed at the beginning of each waveform capture interval.

$>\sim 0.02-0.1$, and the Gaussian half-width was the order of a few λ_D. Note that the untimed structures would have larger potentials and scale sizes. The speeds, scale sizes, and the sign of the potential are consistent with electron holes [*Ergun et al.*, 1998; *Cattell et al.*, 1999].

[9] The relationship of the solitary waves to electron distributions can be seen in Figure 3, which plots sample electron distributions obtained during the waveform captures (note that about three distributions were obtained during each capture). The distributions in Figures 3a and 3b were obtained at a time when solitary waves were observed, whereas the distributions in Figures 3c–3f were obtained during intervals without solitary waves. Solitary waves were observed only at the outer edge of the current sheet when either a narrow electron beam or narrow counter-streaming beams occurred. Although C3 and C4 obtained simultaneous bursts, only C4 observed solitary waves, which occurred in association with a narrow counter-streaming distribution with ~600 eV earthward moving and ~1.5 keV tailward moving electrons (Figure 3a). The beams were cold with $T_{perp} < 100$ eV. When it was closer to the center of current sheet, C4 observed hot, fairly isotropic distributions (Figure 3c). C3 (Figure 3d) observed distributions with very broad pitch angle beams throughout the waveform capture, and no solitary waves were observed. C2 and C1 obtained bursts later. Closest to center of current sheet, C2 observed fairly isotropic distributions and ones that were broad in pitch angle (Figure 3e). Near the end of the burst, C2 observed an intense narrow 5 keV electron beam superimposed on an isotropic distribution (Figure 3b), in association with solitary waves. C1 (Figure 3f) measured isotropic distributions or very broad beams superimposed on an isotropic background throughout its waveform capture and observed no solitary waves.

[10] The density structure of the current sheet crossing on C2, C3, and C4 associated with the waveform captures on C3 and C4 is shown in Figure 4, which plots B_x (black), the density obtained from the spacecraft potential (green), and E_z in the waveform capture (purple) for the two waveform captures. All three satellites encounter a deep density cavity at the outer edge of the current sheet at a distance of ~1500–2000 km from the center. Electron holes are observed only at the end of the waveform capture on C4, as indicated by the brown box, in the region of the density decrease at the outer edge of the current sheet.

[11] The shape of the solitary waves can be inferred, on a statistical basis, from the relative size of the parallel and perpendicular electric fields. The argument can only be made statistically because it is not possible to determine at what distance from the center of the hole (where the perpendicular component would be zero for any shape) the satellite passed through the solitary wave structure. Examples are shown in Figure 5, which plots the two perpendic-

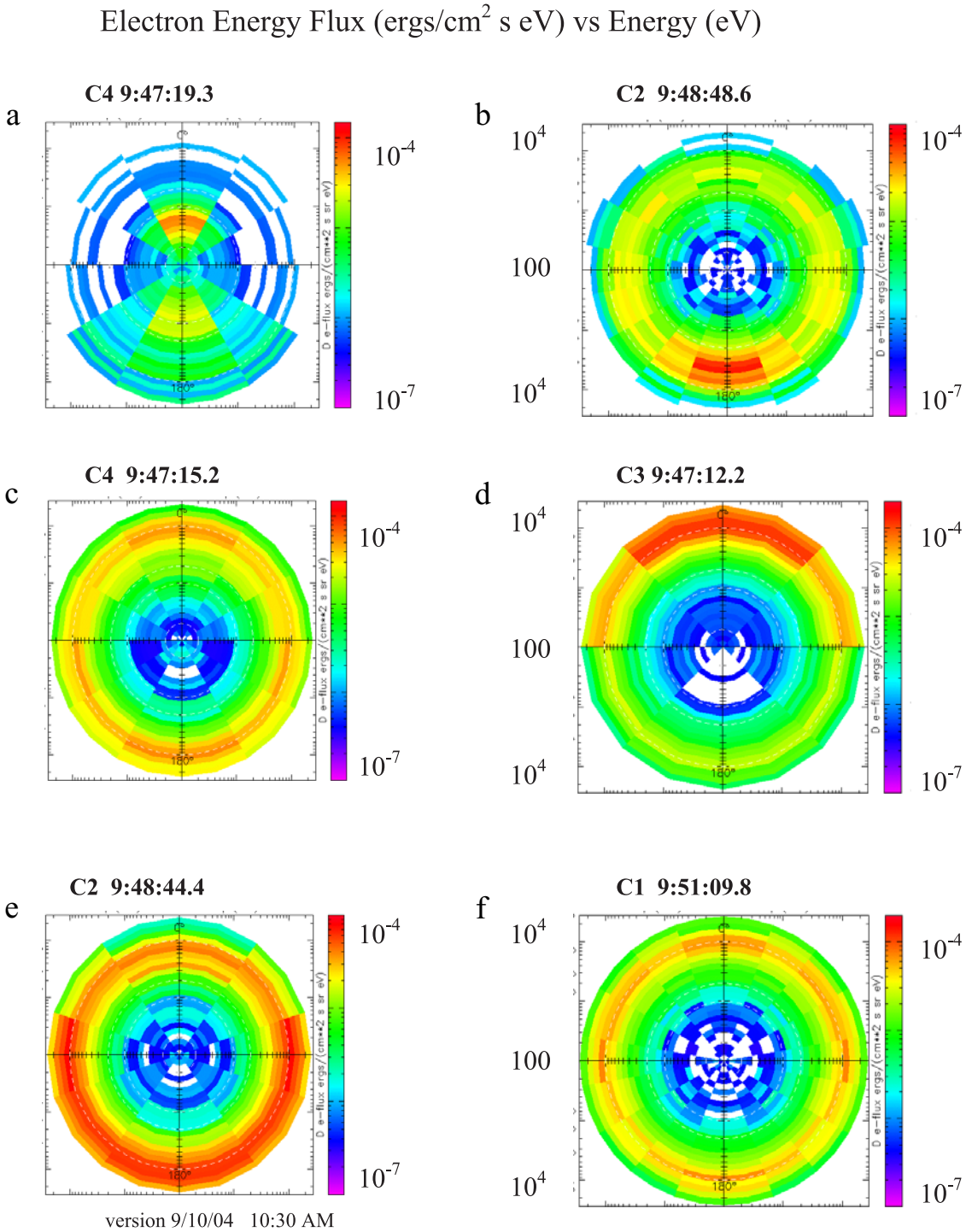

Figure 3. Sample electron pitch angle distributions obtained during intervals (a and b) with and (c–f) without solitary waves. Pitch angle of 0° is at the top of each panel, and 180° is at the bottom. Distributions are in energy flux plotted versus energy from 100 to 10,000 eV.

ular components of the electric field (Ex_fac and Ey_fac) and the parallel component (Ez_fac) in magnetic field-aligned coordinates. Figure 5a (from C2) and 5b (on C4) both show examples where the parallel and perpendicular components are comparable, consistent with a spherical shape. For the example shown in Figure 5c (from C4), the parallel component is larger, consistent with an oblate ellipsoid. In a statistical study of electron holes observed at lower altitudes (<~8 R_E), *Franz et al.* [2000] concluded that electron holes were spherical (comparable parallel and perpendicular components) for $f_{ce}/f_{pe} > \sim 1$ and became more oblate (parallel component larger than perpendicular component) as this ratio became smaller. For both the C2 and C4 waveform capture intervals, $f_{ce}/f_{pe} < 1$, so Franz et al. predict that the parallel component should be much larger than the perpendicular component. This is not con-

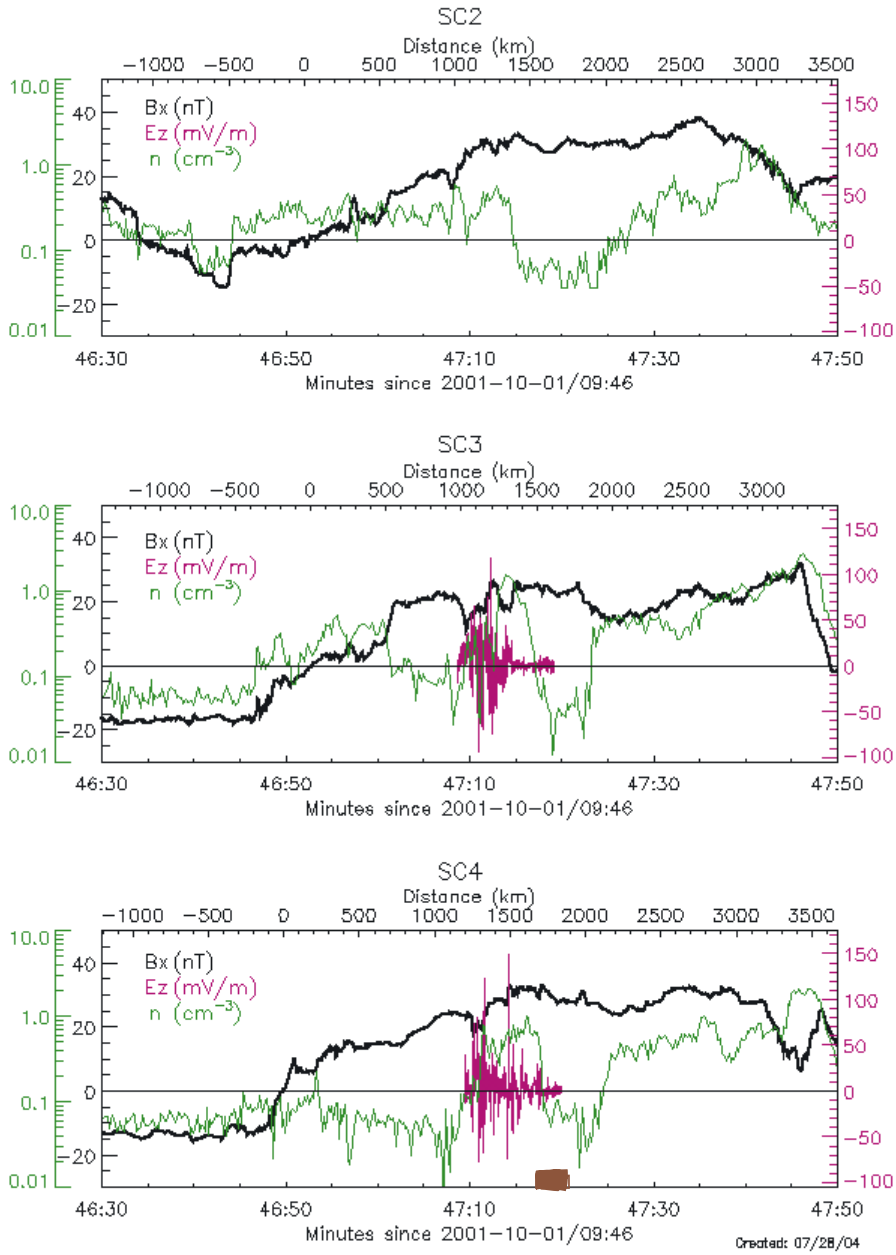

Figure 4. Density structure of the current sheet crossing associated with the C3 and C4 waveform captures. (top) C2, (middle) C3, and (bottom) C4. Each panel plots B_x (black) and the density obtained from the spacecraft potential (green) through the current sheet crossing. E_z in the waveform capture is plotted in purple for the two waveform captures. Region where solitary waves were observed by C4 is indicated with a brown box.

sistent with the observations since only a few solitary waves (such as the case in Figure 5c) have small perpendicular components, and the fact that the on-axis component of the electric field (primarily perpendicular to the magnetic field) is not measured is likely to result in an underestimation of the perpendicular component. However, it is important to remember that this conclusion is limited by the small number of events.

[12] There were several other interesting features in the waveform captures (not shown in the figures). A bipolar electric field pulse parallel to the magnetic field with much longer duration (~0.3 s) and larger amplitude (~150 mV/m) than the solitary waves was seen by C4 at the edge of a unipolar magnetic field perturbation (duration ~0.6 s) of ~7 nT. Such a structure was not seen in the other waveform captures. Whereas the high-frequency waves were usually polarized predominantly parallel to the magnetic field, both C2 and C4 observed some bursts of high-frequency waves polarized perpendicular or oblique to the magnetic field. C2 observed ~10–20 mV/m waves at frequencies of ~4–4.5 kHz oblique to the magnetic field at the beginning of the burst (in association with the broad counter-streaming

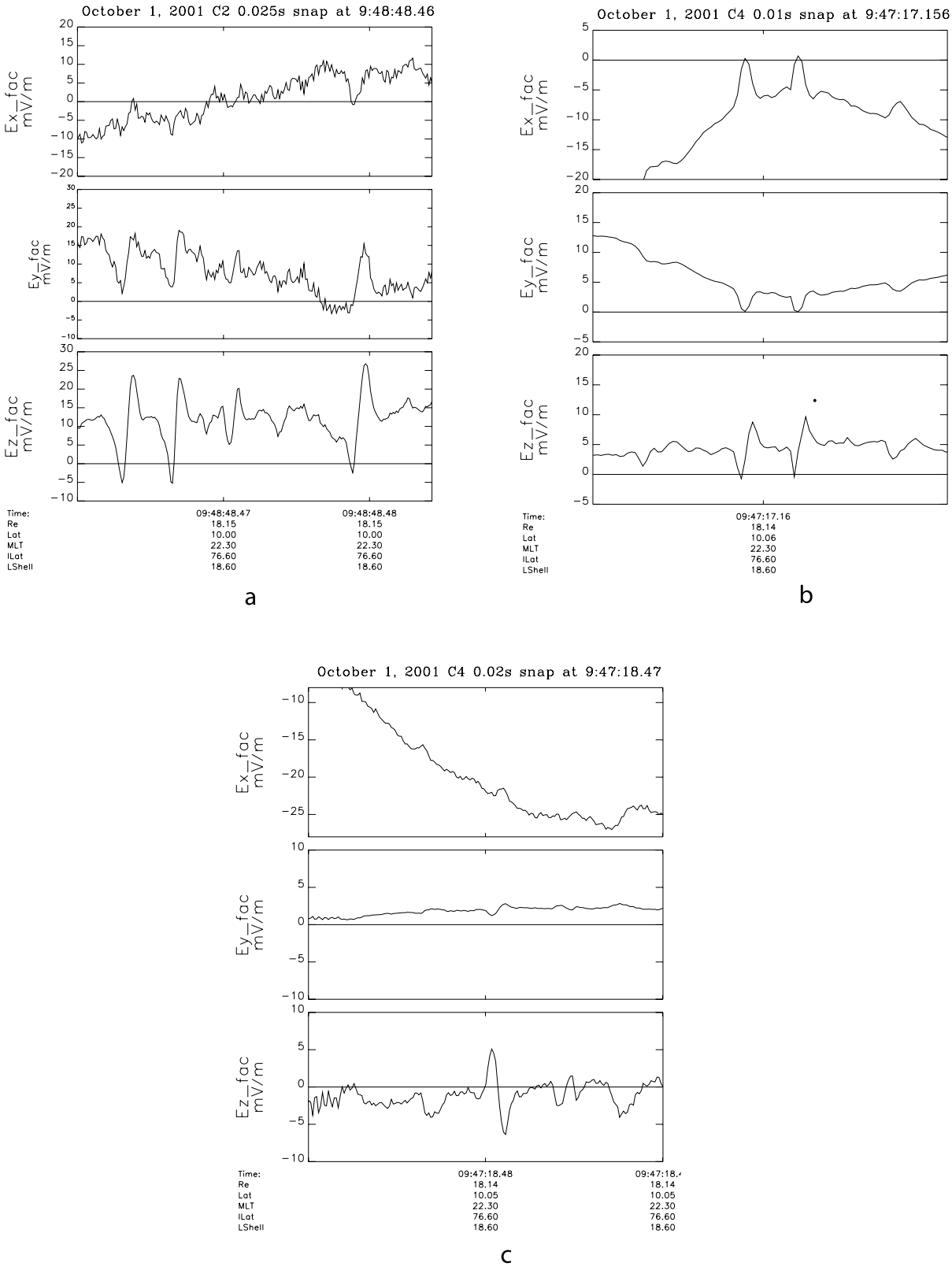

Figure 5. (a, b, and c) Examples of the three components of the electric field in field-aligned coordinates to show the perpendicular signature of the solitary waves. Start time and duration of each sample is given in the title. Note that this rotation into field-aligned coordinates assumes that the on-axis electric field is zero and therefore underestimates the perpendicular component.

beams). At ~0947:17.8, C4 saw a ~10 mV/m burst of waves at ~3.5–4 kHz, which was primarily perpendicular to the magnetic field. It is possible that these waves on C2 and C4 were upper hybrid waves, as previously reported in association with tail reconnection by *Farrell et al.* [2002].

4. Comparison to Simulation Results

[13] Results from particle simulations are presented for comparison to the Cluster data (see *Zeiler et al.* [2002] for discussion of the p3d simulation code). The goal of these simulations is to reproduce the electron distribution functions, including the strong beam features, and the electron holes that are observed in the data. We have not been completely successful in that we have not been able to complete a single simulation that produces the beams and holes with a set of parameters fully consistent with the observations. Specifically we require a somewhat larger initial ambient guide field (0.5 times the reversed field) than can be inferred from the observations (0.2 times the reversed field) to produce electron holes with the spatial distribution, speeds, and structure seen in the Cluster data. We suggest, however, that it is likely that this problem arises because of the limited spatial domain of the simulations (constrained by available computational resources).

[14] The simulations were initialized with a conventional Harris equilibrium with a nonzero lobe density outside of the current sheet and a small, initially uniform guide field B_y. The intent of the simulation is to match the measured tail parameters as closely as possible (within the constraints of required computer time) to try to reproduce the particle distributions and magnetic geometry seen in the observations. Electron beams with a drift speed exceeding the electron thermal speed as seen in the data are produced in the simulations only if the spatial dimensions of the simulation are sufficiently large, typically >20 c/ω_{pi} in the x direction in the usual magnetospheric coordinate system. Three-dimensional simulations of the dynamics of systems of this spatial size cannot be carried out while at the same time maintaining sufficient spatial resolution to describe the electron holes. The simulations are therefore limited to 2-D in the x-z plane in magnetospheric coordinates, which limits the structures and dynamics that can be studied. Nevertheless, the strong in-plane drifts are sufficient to drive electron holes even in this 2-D model. Unless otherwise stated, the simulations were carried out on a 25.6 × 12.8 c/ω_{pi} grid (with 2048 × 1024 grid points), had an initial density ratio between the plasma sheet and the lobe of 10, an electron-ion temperature ratio of 0.1, an electron to ion mass ratio of 0.01, a velocity of light of 20.0 c_A, where c_A is the Alfvén speed (corresponding to $f_{pe}/f_{ce} = 2.0$), and an initial current layer width of 0.25 c/ω_{pi}. The narrow current layer was chosen to speed the development of reconnection, and the results are not sensitive to this value since the results shown are after the lobe plasma has entered the x line. The lobe plasma was represented by 100 particles per cell in the initial state, with correspondingly more particles in the current sheet (totaling in excess of 200 million particles). The simulation was of a double current layer, which allows reconnection to proceed without the stabilizing influence of conducting boundaries. Space and time in the code are normalized to the ion inertial length and the ion cyclotron period so that velocities are normalized to the Alfvén velocity. The particle dynamics are fully relativisitic.

[15] In Figures 6a–6c we show the results of a simulation with a guide field of 0.2 times the reversed field. In Figure 6a the x component of the electron flow velocity in the x-z plane and the electron velocity distributions at representative locations are shown. Only one quadrant of the simulation is shown so that the detailed structure of the x line can be more clearly seen. The large center panel is the x component of the electron flow velocity in the x-z plane, and the smaller panels are the electron velocity distributions in the v_x-v_z (top) and v_x-v_y (bottom) planes at the numbered locations indicated. The solid lines in these smaller panels indicate the direction of the local magnetic field. The electron velocity plot shows an asymmetric pattern of alternating inflow and outflow. The six distributions shown in Figure 6a provide a representative sample of the types of distributions that occur. The velocities are normalized to the Alfvén speed (based on the initial upstream magnetic field and plasma sheet density), and the phase space density scale varies from plot to plot. Position 6, the upstream "lobe" plasma, has a cold slightly anisotropic distribution that is inflowing in the $+z/+x$ direction toward the x line. At position 5 a distinct beam has formed that is nearly field aligned and flowing toward the x line. The drift speed of this beam depends strongly on the ratio of the density in the central current layer to that in the lobe, the strength of the initial value of B_y, and the size of the computational domain. Larger values of B_y and larger simulation scale sizes produce stronger beams. The beams seen in this 25.6 × 12.8 c/ω_{pi} simulation are stronger than those seen in a 12.8 × 6.4 c/ω_{pi} simulation. Our expectation is that a computational domain larger than that shown in Figures 6a–6c would produce an even stronger beam, although this has not been verified. At position 2, just upstream of the x line, the flow is in the negative z direction and is very anisotropic with $T_{par} > T_{perp}$. The reduction in T_{perp} is a consequence of the conservation of magnetic moment as particles move into regions of smaller magnetic field. The distribution at position 3, obtained at the x line where the magnetic field is very small, contains two distinct beam components. The most energetic particles are preaccelerated along acceleration zones (discussed more fully later in this section) along the upper left and lower right separatrices before moving into the x line acceleration zone. The weaker beam consists of particles that directly enter the x line. Position 4 is the distribution from the outflow region just downstream of the separatrix. Evident are two distinct components, a hot outflowing electron beam that was ejected from the x line and a cold beam that crossed the separatrix. The most processed plasma is at position 1, near the center of the current sheet. The distribution has been heated and isotropized and has the highest density, as is seen in the central plasma sheet of the Cluster data.

[16] In Figures 6b and 6c the log of the density and the electron parallel velocity are plotted over the entire x-z plane. The pale yellow regions in Figure 6b are density cavities [*Kleva et al.*, 1995; *Tanaka*, 1996; *Pritchett and Coroniti*, 2004] that result as the electrons, accelerated by the parallel electric field, move with high velocity toward the x line, effectively draining the separatrix region of electrons. Electrons are ejected from the x line along the separatrix on the opposite side of the current layer, breaking

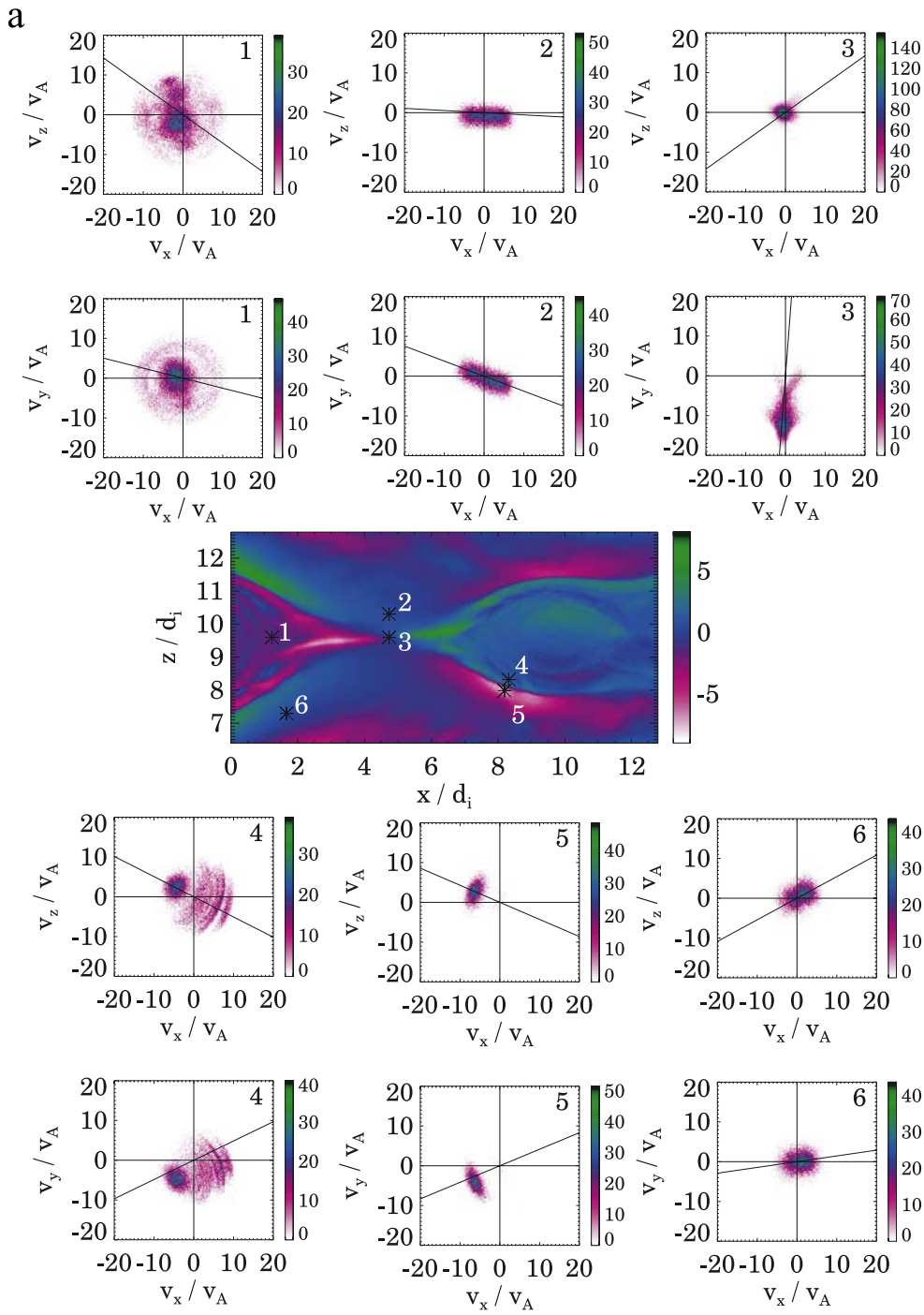

Figure 6. (a) Sample electron phase space distribution functions in (top) *vz-vx* and (bottom) *vy-vz* at the numbered locations in the center panel, which plots the *x* component of the electron flow velocity in the *x-z* plane from a two-dimensional (2-D) particle simulation of reconnection with guide field of 0.2. (b) Plasma density in the *x-z* plane. (c) Parallel electron velocity in the *x-z* plane. Note that only one quadrant of the simulation domain is shown in Figure 6a so that the structure is more visible. Electron velocity is normalized to the initial Alfvén speed and distances to the ion inertial length.

the symmetry that exists in the case with no ambient guide field. The resulting perpendicular electric field expels the ions so that a similar plot for the ions also reveals these cavities. In Figure 7 we show cuts of the electron density across the current layer for a case with no ambient guide field (dashed) along with the case with a guide field of 0.2 (solid). With a guide field one cavity becomes much deeper than without a guide field, and the other is filled in. The cavity becomes even deeper with a larger guide field. These cavities were also present in previous simulations of electron holes [*Drake et al.*, 2003]. The data from Cluster, shown in Figure 4, are suggestive of deep cavities at the

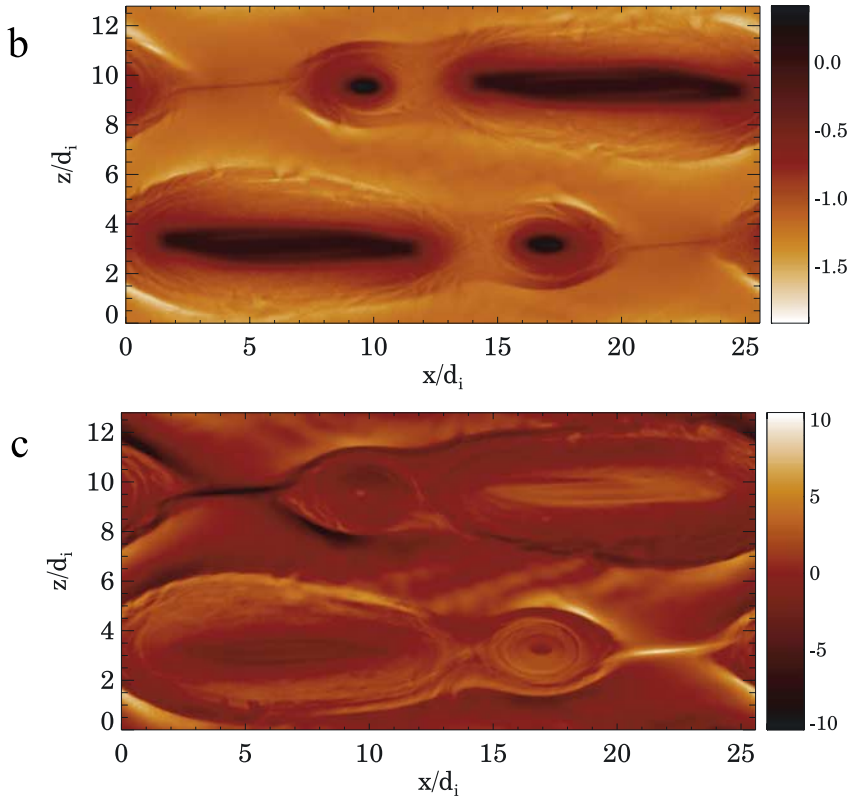

Figure 6. (continued)

outer edge of the plasma sheet, which can be interpreted as further evidence that there is a nonzero guide field in the reconnection event seen in the Cluster data. In Figure 6c we show the electron parallel velocity again for the case of 0.2. The highest streaming velocities occur in the density cavities of Figure 6b with peak values around 10, consistent with the beam speed of 8 shown in the distributions at location 4 in the cavity of Figure 6a. These beams, because of the small value of the ambient B_y, flow mostly in the z-x plane.

[17] The strong electron flows present in the density cavities along with the ambient density gradients drive short-scale fluctuations, but these do not develop into spatially localized electron holes and are not even clearly related to the Buneman instability seen in earlier 3-D simulations [*Drake et al.*, 2003]. We believe, however, that a simulation with the same ambient guide field but in a larger computational domain would increase the electron streaming velocity in the density cavities and would very likely produce electron holes. The strong electron streaming seen in Figure 6c results from the acceleration of the electrons in a parallel electric field that remains finite along the length of the density cavity and therefore along the entire separatrix. The peak electron velocity and beam speed is therefore linked to the length of the acceleration region or the length of the computational domain. Thus far, we have not seen a cutoff of the length of the acceleration cavity independent of the length of the computational domain.

[18] Because of limitations in available computer time, increasing the box size further is not an option. As an alternative we have carried out simulations identical to those shown in Figures 6a–6c but with the ambient guide field increased to 0.5. The increased guide field causes electrons to move a greater distance in the y direction for a given distance in x, thus effectively increasing the length of the acceleration cavity for a given computational box length L_x. In Figure 8 we compare the distribution functions in the v_y-v_x plane obtained at position 5 from simulations with a guide field of 0.2 (top) and 0.5 (bottom). The increased guide field increases the beam speed from around 8 for the case of 0.2 to around 12 for the case of 0.5. Note also that the effective temperature of the stronger beam has gone down. This cooling effect is a well-known phenomenon in

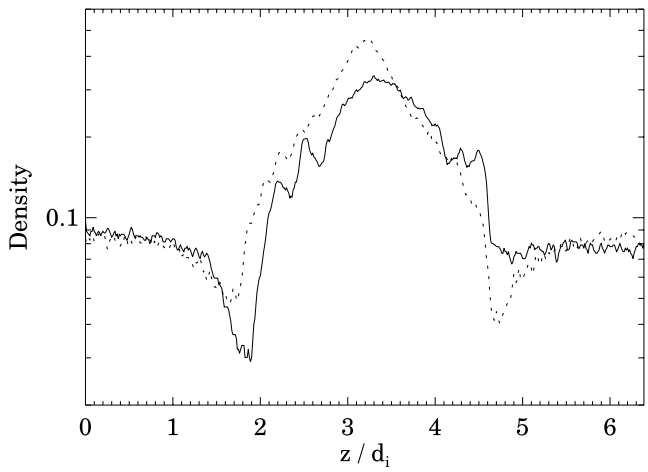

Figure 7. Cuts of the electron density across the current layer for a case with no ambient guide field (dashed) along with the case with a guide field of 0.2 (solid).

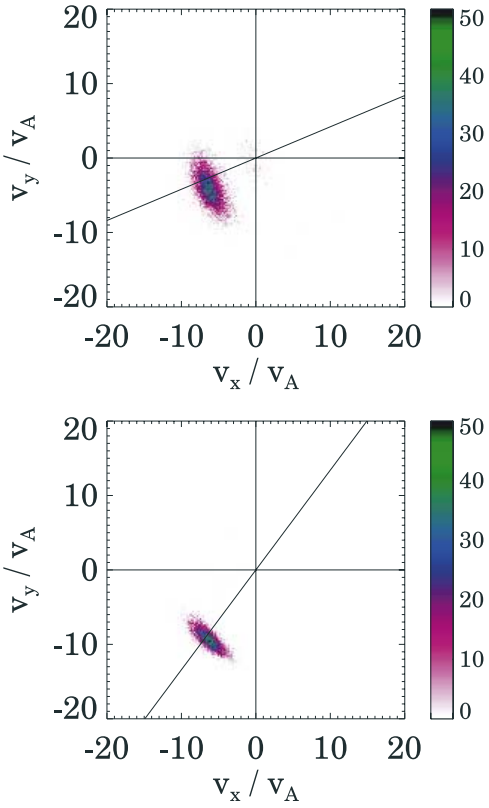

Figure 8. Electron distribution functions in the v_y-v_x plane obtained at position 5 from simulations with a guide field of (top) 0.2 and (bottom) 0.5. Beam is stronger in the guide field of 0.5 case.

the literature on particle accelerators. Shown in Figures 9a and 9b are plots of the parallel electron velocity and parallel electric field for the case with 0.5 guide field, taken at t = 10.4 ω_{ci}^{-1}. Consistent with the distribution function for this case shown in Figure 8, the electron streaming velocity has now increased compared with Figure 6c. The parallel electric field in Figure 9b reveals large-scale structure and instabilities at two distinct scales, the smallest taking the form of localized bipolar structures (adjacent regions of black and pale yellow) consistent with the structure of observed electron holes. The extended regions of positive and negative parallel electric field map onto the density cavities (analogous to those shown for the case of guide field 0.2) and the large parallel streaming velocities correspond to the regions of extended large values of the parallel electric field. The electron holes are, surprisingly, scattered over a range of spatial locations. These bipolar structures are positively charged and are associated with depletions in the local electron density. The ion density perturbations associated with the holes are much smaller. The absence of holes near the x line is because in this region the in-plane magnetic field is small and the electron velocity is dominantly in the y direction and therefore not unstable in the 2-D model. In a full 3-D simulation (not possible for the large simulation domain shown) the electron holes should also develop close to the x line as demonstrated by *Drake et al.* [2003]. The dispersal of electron holes within the magnetic islands in Figure 9b may not be representative of physical reality. The electrons have sufficient velocity (up to 15) to spiral around the island several times during the duration of the simulation. Evidence for this behavior can be seen inside of the large island in the upper right hand corner of Figure 9a. It is likely that this spiraling electron beam is driving the holes seen in Figure 9b. During a large-scale reconnection event in the tail such spiraling would probably not be as prominent, and we would not expect the holes to be measured well inside of the magnetic separatrix unless plasmoids of sufficiently small scale develop. The mobility of electrons in the x direction can be inhibited by increasing the guide field since the parallel electron velocity will be further tilted in the y direction. In Figure 10 we show the parallel electric field from a simulation with a guide field of 1.0. This simulation was in a somewhat larger computational domain (32 $\times$ 16 c/ω_{pi}) with a central to lobe density ratio of 5.0. A chain of electron holes has developed around the separatrices of the magnetic islands in the locations of the density cavities analogous to those shown in Figure 9b. The location of the holes is consistent with the Cluster observations, in which the holes are often observed at the boundary of the plasma sheet where the plasma density plunges sharply into a low-density cavity. These localized nonlinear structures develop only relatively late in the simulation after the reconnection-driven beams become strong. They evolve from periodic fluctuations, grow to large amplitude with the largest-amplitude fluctuations coalescing into the localized structures evident in Figure 10a. The holes in this simulation have velocities around 3.0, much smaller than the electron streaming velocity, which peaks around 15. The relatively low hole speed is consistent with the Buneman instability as the underlying source and is consistent with the results of earlier 3-D simulations and the observations. Shown in Figure 10b is the structure of the parallel electric field along a contour that follows a magnetic field line in the z-x plane through the region of largest hole amplitude. This contour is marked with the solid black line in Figure 10a. The characteristic bipolar signature in the parallel electric field indicates the presence of a number of electron holes. As is also seen in the Cluster observations, some holes are asymmetric and therefore sustain a net potential drop.

[19] The dynamics of the turbulence shown in Figures 9 and 10, including the drive mechanism, will be explored more fully in a separate publication. The goal of the present set of figures and discussion is to show that electron beams and electron holes consistent with the Cluster observations require a small ambient guide field to develop but that the required guide field may be small and therefore not inconsistent with the observational data.

[20] Using the simulation results to provide a framework for examining the structure and dynamics of the plasma sheet during this interval as seen at the four Cluster satellites, the relationship of electron holes to reconnection is investigated in more detail. This will also allow us to infer the regions where electron holes would be observed if there were continuous waveform captures. During the time period when C3 and C4 obtained waveform captures, all four satellites remained north of and moved away from the center of the current sheet; C3 (C1) was closest to (farthest from) the center of the current sheet, and C2 and C4 were at similar distances from the center. C3 was closest to the

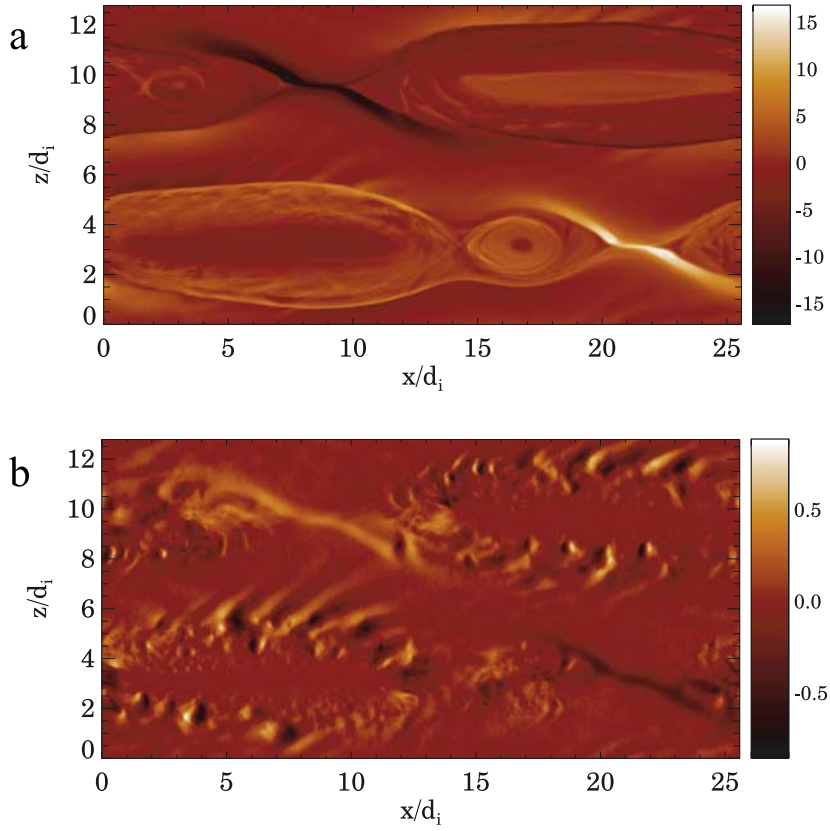

Figure 9. Results from the 2-D simulation with guide field of 0.5. (a) Parallel electron velocity in the *x*-*z* plane. (b) Parallel electric field in the *x*-*z* plane.

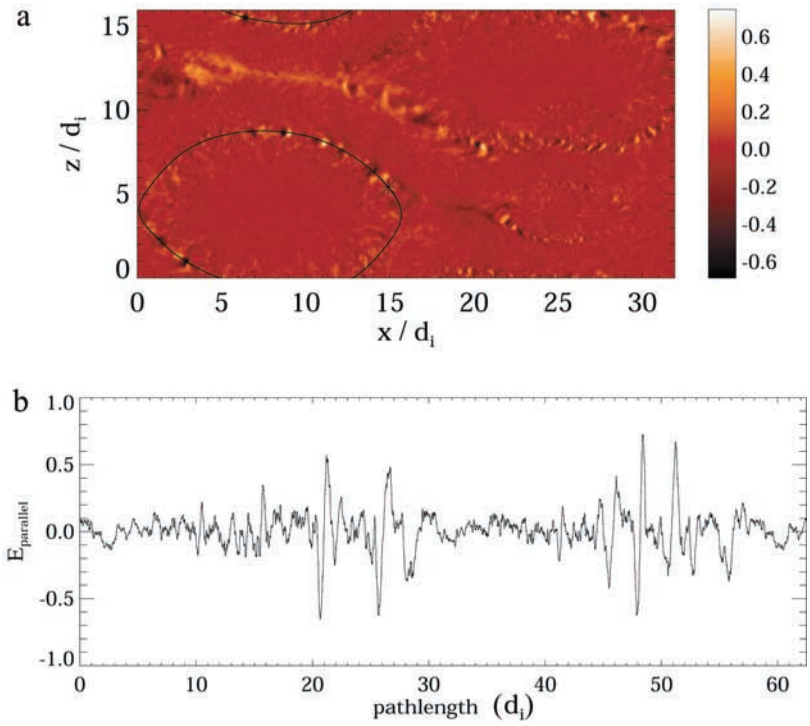

Figure 10. Results from the guide field of 1.0 case. (a) Parallel electric field in the *x*-*z* plane. (b) Parallel electric field along the black line shown in Figure 10a. Typical bipolar signature of electron holes is clearly visible.

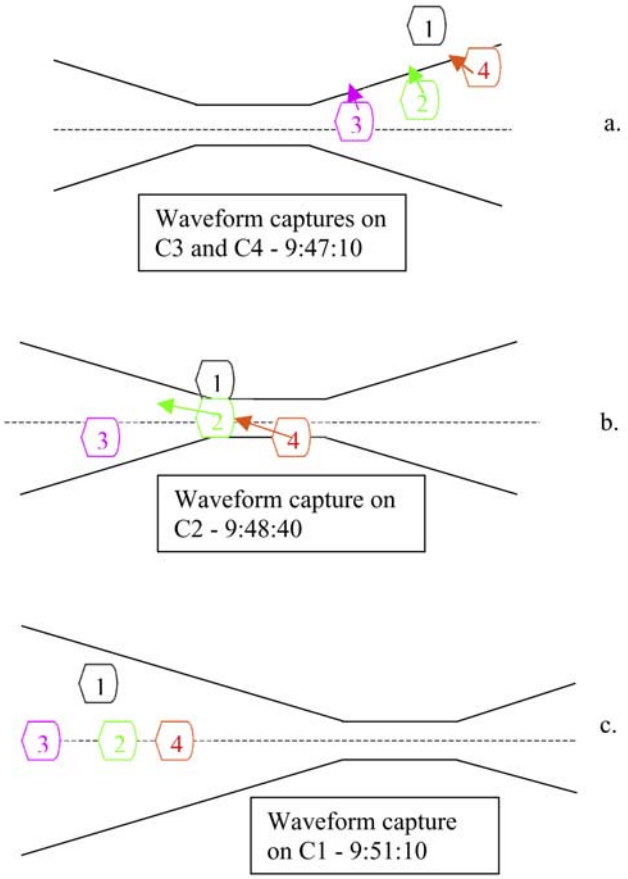

Figure 11. Cartoon of relative locations of Cluster satellites and the reconnection x line (not to scale) for time of (a) C3/C4 waveform capture, (b) C2 waveform capture, and (c) C1 waveform capture.

Earth and was the first satellite to see the onset of tailward flow and the subsequent switch to earthward flow. The relative locations of the satellites and the reconnection x line is sketched in Figure 11a. The distributions observed by C1 were similar to positions 2 and 6 in Figure 6a. The first two pitch angle distributions obtained by C4 during the waveform capture, when it was closest to the center of the current sheet, were hot and fairly isotropic (similar to position 1 in Figure 6a). Solitary waves occurred only when narrow intense counter-streaming beams were observed at a distance of >1600 km from the center of the current sheet at ~0947:19. C3, which only reached a distance of ~1500 km above the current sheet, observed distributions with very broad pitch angle beams throughout the waveform capture (intermediate between the type at position 1 and position 5 in Figure 6a). The distribution obtained at the greatest distance during the waveform capture on C3 consisted of a narrow weak beam in tailward direction and a hot, very broad earthward beam. Although nonlinear waveforms at high frequencies (~1–2.5 kHz) occurred, there were no solitary waves. At 0947:16, within the density cavity (see Figure 4), C2 observed narrow low-energy counter-streaming beams, almost identical to those seen by C4 at 0947:19. It is likely that electron holes would have been observed by C2 at this time. Prior to this distribution (closer to the current sheet) the distributions at C2 were isotropic (as at position 1), and electron holes would not be expected to occur.

[21] At the time of C2 waveform capture (see Figure 11b), C2 was north of the center of the current sheet, C1 was northward of C2, and C4 moved northward across the center right after the start of the waveform capture but remained closer to the center than C2. C3 was primarily south of or close to the center of the current sheet. C3 was earthward of the x line, in the region of earthward flow throughout the C2 capture; C4 observed the switch to earthward flow near the middle of the capture interval at ~0948:43. The C2 waveform capture was therefore obtained earthward of and much closer to the x line than the C3/C4 waveform captures. At ~0948:36, just prior to the beginning of the waveform capture, C2 observed a cold tailward beam and a hot very broad earthward beam. At ~0948:40 both were broadened, and the earthward portion of the distribution was more intense consistent with distribution 4 in Figure 6a, the next was a more isotropic distribution, and finally, at a distance of >~1500 km from the current sheet center, an intense narrow tailward beam at 5 keV superimposed on a hot isotropic background was observed at ~0948:48 and again at 0948:52 (similar to the distributions at position 3 or 4 in Figure 6a). The observation of a more isotropic distribution in the second distribution is consistent with the fact that motion of the current sheet resulted in C2 being closer to the center during that interval. Solitary waves were seen only in association with the narrow beam at the end of the capture. C4 measured a similar energetic beam at ~0948:54. Closer to the current sheet center at 0948:33, there was a narrow lower-energy earthward beam and hotter very broad distribution on the tailward side. C3 saw the same thing at 0948:30, just after switch to earthward flow, and continued to observe counterstreaming beams for the next two distributions. Throughout the interval of the C2 capture, C1 saw narrow low-energy counter-streaming beams very similar to those observed by C4 at the time solitary waves occurred. These observations suggest that if the waveform capture data had been taken during this interval, all four satellites would have observed solitary waves during parts of the time period.

[22] The C1 waveform capture occurred when all four satellites were within the plasma sheet in the region of earthward flow (see Figure 11c), after the tailward retreat of the reconnection x line. All the satellites observed isotropic distributions (similar to position 1 in Figure 6a) and/or very broad hot beams. No solitary waves were observed by C1, and none would be expected to occur at the positions of the other satellites.

[23] Examination of the distributions on all four satellites indicates that electron holes are excited in the separatrix region, near the outer edge of the current sheet, where there are narrow electron beams, either unidirectional or counter-streaming. The region containing the beams (and therefore the electron holes) can extend over thousands of kilometers in the x and y directions but is very narrow in the z direction. This is consistent with the simulation results. C2 and C4 (separated by ~500 km in Z_{gse}) were often at the same distance above the current sheet center and observed very similar features in the electron distributions at end of the C3/C4 and C2 bursts. C2 was more duskward and earth-

ward than C4. In both cases there was a delay a few seconds with C4 seeing the feature later. We speculate that the narrow electron beams were seen over a larger volume during the C2 waveform capture interval because all the satellites were closer to the x line (as indicated by the ion flow reversal times). During this interval, electron holes would likely have been observed at times by all four satellites, so that electron holes would occur over a large volume. During the C3/C4 capture interval, when all four satellites were farther from the x line, electron holes would be observed only by the two satellites within the separatrix (C2 and C4).

5. Discussion and Conclusions

[24] The Cluster satellites have, for the first time, observed large-amplitude solitary waves at multiple locations along the separatrices associated with tail magnetic reconnection as the x line passed tailward over the satellites and have shown the one-to-one correlation between the existence of narrow electron beams and solitary waves. These observations have also provided the first measurements of the velocity, scale size, and amplitude of solitary waves in the magnetotail outside the $\sim 9\ R_E$ orbit of Polar. The solitary waves properties are consistent with electron holes. Because of instrumental limitations the association with narrow electron beams has previously been observed only in the low-altitude auroral zone [*Ergun et al.*, 1998]. Very large-amplitude ($\sim$100 to >250 mV/m) waves near the lower hybrid frequency were seen on all four Cluster satellites in four different locations. The lower hybrid amplitudes are 1–2 orders of magnitude larger than previously reported in association with reconnection [*Cattell and Mozer*, 1986; *Cattell et al.*, 1995; *Bale et al.*, 2002; *Shinohara et al.*, 1998].

[25] Comparisons of 3-D particle simulations of reconnection to Polar magnetopause observations were presented by *Drake et al.* [2003]. This study showed that the electron holes, which developed in the region of the electron beams, initially at the x line and then along the separatrices, were due to the nonlinear growth of the Buneman instability and had speeds on the order of a tenth of electron beam speed, comparable to the Buneman phase velocity and much less than the electron beam velocity. The growth of the holes was strongly controlled by the dynamics of lower hybrid waves that had wave vectors primarily transverse to the direction of the initial guide field. Electron holes occurred in the diffusion region, producing substantial electron-ion scattering, and along the separatrices. The holes had an important role in the dynamics of the reconnection process and the associated dissipation and particle energization. Although the *Drake et al.* [2003] simulations used a large guide field (B_y for the magnetotail), a recent study (M. Swisdak et al., The transition from anti-parallel to component magnetic reconnection, submitted to *Journal of Geophysical Research*, 2004) shows that $B_{\rm guide}/B_{\rm reversing} \sim 0.1$ is large enough so that the electrons remain magnetized and escape from the x line before being strongly heated, and unstable electron distributions develop, as can also be seen in the results presented herein in Figures 6a–6c. Earlier large scale-size simulations [*Swisdak et al.*, 2003] indicate that current and electron drift are large for hundreds of $c/\omega_{\rm pi}$ from the x line along separatrices, not just close to x line, so that the signatures of electron holes should be observable over a large volume. This was confirmed by the simulations shown in Figure 10, which showed that electron holes were excited along the separatrices.

[26] Simulations with density gradients and smaller guide fields (consistent with observations of the magnetosphere) cannot reproduce the full evolution of the holes due to computational limitations (for smaller guide magnetic fields, large computational domains are required to produce intense beams). The Polar observations of electron holes at the magnetopause were consistent with the predictions from the 3-D simulations; however, the Polar plasma instrument did not make high enough time resolution measurements, and the expected electron beams were not observed. The Cluster PEACE instrument contains a mode that is able to obtain higher time resolution measurements of distributions, and the data described herein showed that the electron holes were only observed during intervals when there were narrow electron beams. The results of several 2-D particle simulations performed to compare with the Cluster observations of electron beams and electron holes during the 1 October 2001 reconnection event were described in section 4. On the basis of the results of the earlier 3-D simulations we expect that these 2-D simulations cannot model the complete dynamics and evolution of the electron holes. In particular, waves that have wave vectors primarily along the guide field direction will not be excited, and electron holes cannot occur in the magnetic field reversal region. However, the 2-D simulations showed that reconnection in systems with realistic density gradients and small guide fields produces electron beams in density cavities that can excite waves that develop into electron holes along the separatrices, consistent with the Cluster observations.

[27] Many features of the magnetotail reconnection event shown herein are in agreement with *Drake et al.* [2003]. Positive potential structures consistent with electron phase space holes were observed in the regions predicted by the simulations, i.e., along the separatrix in association with narrow electron beams. The measured velocity, scale sizes, and circular shape of the holes match those obtained from the simulations. The predicted hole speed, v_h, is approximately equal to $(m_e/m_i)^{1/3} v_{\rm de}$, where $v_{\rm de}$ is the electron beam speed. This prediction is $\sim$900–3500 km/s, compared to the observed speeds of $\sim$700 to >2500 km/s. The predicted hole scale size $L_h = v_{\rm de}/f_{\rm pe} \sim 4$–14 km, compared to the observed $>\sim$3 km. The largest-amplitude electron holes occurred in the event with the most energetic electron beam. Large-amplitude waves near the lower hybrid frequency and polarized perpendicular to the magnetic field were associated with electron holes. In the regions where electron holes were seen, their amplitudes were comparable to or less than the amplitudes of the lower hybrid waves, consistent with Drake et al., who showed that hole evolution is controlled by the growth of large-amplitude (perpendicular) lower hybrid waves. The role of lower hybrid waves in the evolution of electron holes has also been examined by *Umeda et al.* [2002] for magnetotail parameters and by *Singh* [2002], *Miyake et al.* [2000], and *Oppenheim et al.* [2001] for auroral zone parameters.

[28] Comparisons of the observed wave modes to simulation studies on the excitation of electron holes in the

magnetotail [*Omura et al.*, 1994, 1996; *Miyake et al.*, 2000; *Umeda et al.*, 2002] can also be made, although the parameters in the simulations are not identical to those observed in this event. The electron distribution observed by C2 during the interval with solitary waves was an intense 5 keV electron beam superimposed on a warm isotropic electron population, which could be modeled as a "bump-on-tail" or a warm bistream, in the classification used by *Omura et al.* [1996]. For both distribution types, *Omura et al.* [1996] found that solitary waves were excited, with Langmuir waves for the bump-on-tail and with waves in the range of $\sim 0.05 < f/f_{pe} < 0.4$ for the warm bistream. C2 observed large amplitude solitary waves and waves at $\sim 0.1\ f_{pe}$, which is most consistent with the warm bistream. C4 observed smaller-amplitude solitary waves and waves at $\sim 0.5-0.7\ f_{pe}$, in association with a counter-streaming electron beam distribution, which could possibly be classified as a "cold bistream." In the cold bistream case, *Omura et al.* [1996] found that a broad spectrum of waves ($\sim 0.1-0.7\ f_{pe}$) was linearly unstable, and solitary waves did develop. The Cluster electron hole speeds, however, are much lower than would be predicted by the Omura simulations, and the wave amplitudes are much larger. Timing of the electron holes observed by Cluster yields speeds that are consistent with the Buneman instability (the order of a tenth of the beam velocity); however, only a small fraction of the observed holes can be timed due to limitations in the instrument, including the fact that the measurement is only 2-D and including the low sample rate ($\sim$16,000 samples/s). No measurable time delay is equivalent to a speed faster than $\sim$2500 km/s. (Note that most of the electron holes observed by Polar at the magnetopause could be timed and were moving at speeds consistent with a fraction of expected beam speeds.) The Cluster and Polar speeds are consistent with an electron-ion streaming instability, as inferred from the *Drake et al.* [2003] simulations. In addition, *Miyake et al.* [1998] did not see solitary wave growth when the ratio f_{ce}/f_{pe} was <0.2, whereas the solitary wave events described herein occurred when this ratio was the order of 0.04–0.1.

[29] We have described observations of large-amplitude solitary waves and other wave modes during magnetotail current sheet crossings associated with passage of a reconnection x line. Although waveform captures were not obtained in the electron diffusion region, they were obtained in the separatrix layer, with examples both earthward and tailward of the x line. Three-dimensional simulations show that the electron holes also occur in the diffusion region. The good agreement between the Cluster data and the predictions of reconnection simulations shown herein and by *Drake et al.* [2003] suggest that the observed microphysics, including electron holes and large-amplitude waves, may play an important role in dynamics of reconnection in the magnetosphere and, in particular, in the evolution of the electron distributions. The fact that similar observations have been made at the magnetopause suggests that microphysics is critical to an understanding of reconnection throughout the magnetosphere.

[30] **Acknowledgments.** The authors thank the Cluster engineering and software teams. C. Cattell thanks the University of Minnesota for sabbatical support and Goddard Space Flight Center and the University of Maryland for their hospitality during the writing of this paper. We thank H. Reme at CESR and the CDAWeb for use of the ion moments. This work was supported by NASA grants NAG5-11944 and NAG5-11124 at the University of Minnesota and NASA grants NAG513052 and NAG512276 and NSF grant PHY-0316197 at the University of Maryland.

[31] Arthur Richmond thanks Philip L. Pritchett and another reviewer for their assistance in evaluating this paper.

References

Bale, S. D., F. S. Mozer, and T. Phan (2002), Observation of lower hybrid drift instability in the diffusion region at a reconnecting magnetopause, *Geophys. Res. Lett.*, *29*(24), 2180, doi:10.1029/2002GL016113.

Balogh, A., et al. (2001), The Cluster magnetic field investigation: Overview of inflight performance and initial results, *Ann. Geophys.*, *19*, 1207.

Birn, J., et al. (2001), Geospace Environmental Modeling (GEM) Magnetic Reconnection Challenge, *J. Geophys. Res.*, *106*, 3715.

Cattell, C. A., and F. S. Mozer (1986), Experimental determination of the dominant wave mode in the active near-Earth magnetotail, *Geophys. Res. Lett.*, *13*, 221.

Cattell, C., et al. (1995), ISEE-1 and Geotail observations of low-frequency waves at the magnetopause, *J. Geophys. Res.*, *100*, 11,823.

Cattell, C., et al. (1999), Comparisons of Polar satellite observations of solitary wave velocities in the plasma sheet boundary and the high altitude cusp to those in the auroral zone, *Geophys. Res. Lett.*, *26*, 425.

Cattell, C., J. Crumley, J. Dombeck, J. Wygant, and F. S. Mozer (2002a), Polar observations of solitary waves at the Earth's magnetopause, *Geophys. Res. Lett.*, *29*(5), 1065, doi:10.1029/2001GL014046.

Cattell, C., J. Dombeck, J. Wygant, F. S. Mozer, and M. André (2002b), The role of waves in magnetotail dynamics, in *Proceedings of the Sixth International Conference on Substorms, Seattle, Washington, March 25–29, 2002*, edited by R. M. Winglee, pp. 443–449, Univ. of Wash., Seattle, Washington.

Dombeck, J., C. Cattell, J. Crumley, W. Peterson, H. Collin, and C. Kletzing (2001), Observed trends in auroral zone ion solitary wave structure characteristics using data from Polar, *J. Geophys. Res.*, *106*, 19,013.

Drake, J., M. Swisdak, C. Cattell, M. Shay, B. Rogers, and A. Zeiler (2003), Formation of electron holes and particle energization during magnetic reconnection, *Science*, *299*, 834.

Ergun, R., et al. (1998), FAST satellite observations of large-amplitude solitary wave structures, *Geophys. Res. Lett.*, *25*, 2041.

Farrell, W. M., M. D. Desch, M. L. Kaiser, and K. Goetz (2002), The dominance of electron plasma waves near a reconnection *X*-line region, *Geophys. Res. Lett.*, *29*(19), 1902, doi:10.1029/2002GL014662.

Franz, J., P. Kintner, and J. Pickett (2000), On the perpendicular scale size of electron phase space holes, *Geophys. Res. Lett.*, *27*, 169.

Gustafsson, G., et al. (1988), The spherical probe electric field and wave experiment, in *The Cluster Mission—Scientific and Technical Aspects of the Instruments*, *ESA SP-1103*, p. 31, ESA Publ. Div., Noordwijk, Netherlands.

Johnstone, A. D., et al. (1997), PEACE: A Plasma Electron and Current Experiment, *Space Sci. Rev.*, *79*, 351.

Kleva, R., J. F. Drake, and F. L. Waelbroeck (1995), Fast reconnection in high temperature plasmas, *Phys. Plasmas*, *2*, 23.

Matsumoto, H., X. H. Deng, H. Kojima, and R. R. Anderson (2003), Observation of electrostatic solitary waves associated with reconnection on the dayside magnetopause boundary, *Geophys. Res. Lett.*, *30*(6), 1326, doi:10.1029/2002GL016319.

Miyake, T., Y. Omura, H. Matsumoto, and H. Kojima (1998), Two-dimensional computer simulations of electrostatic solitary waves observed by Geotail spacecraft, *J. Geophys. Res.*, *103*, 11,841.

Miyake, T., Y. Omura, and H. Matsumoto (2000), Electrostatic particle simulations of solitary waves in the auroral region, *J. Geophys. Res.*, *105*, 23,239.

Omura, Y., H. Kojima, and H. Matsumoto (1994), Computer simulation of electrostatic solitary waves: A nonlinear model of broadband electrostatic noise, *Geophys. Res. Lett.*, *21*, 2923.

Omura, Y., et al. (1996), Electron beam instabilities as the generation mechanism of electrostatic solitary waves in the magnetotail, *J. Geophys. Res.*, *101*, 2685.

Oppenheim, M., G. Vetoulis, D. Newman, and M. Goldman (2001), Evolution of electron phase-space holes in 3D, *Geophys. Res. Lett.*, *28*, 1891.

Parker, E. N. (1957), Sweet's mechanism for merging magnetic fields in conducting fluids, *J. Geophys. Res.*, *62*, 509.

Pedersen, A. (1995), Solar wind and magnetospheric plasma diagnostics by spacecraft electrostatic potential measurements, *Ann. Geophys.*, *13*, 118.

Petschek, H. E. (1964), Magnetic field annihilation, *NASA Spec. Publ.*, *SP-50*, 425.

Pritchett, P. L., and F. V. Coroniti (2004), Three-dimensional collisionless magnetic reconnection in the presence of a guide field, *J. Geophys. Res.*, *109*, A01220, doi:10.1029/2003JA009999.

Runov, A., et al. (2003), Current sheet structure near magnetic *X*-line observed by Cluster, *Geophys. Res. Lett.*, *30*(11), 1579, doi:10.1029/2002GL016730.

Shinohara, I., et al. (1998), Low-frequency electromagnetic turbulence observed near the substorm onset site, *J. Geophys. Res.*, *103*, 20,365.

Singh, N. (2002), Temporal and spatial features of waves and electron holes driven by double layers and their relevance to VLF saucers, *Geophys. Res. Lett.*, *29*(17), 1833, doi:10.1029/2002GL015195.

Sweet, P. A. (1958), Electromagnetic phenomena, in *Cosmical Physics*, p. 123, Cambridge Univ. Press, New York.

Swisdak, M., et al. (2003), Diamagnetic suppression of component magnetic reconnection at the magnetopause, *J. Geophys. Res.*, *108*(A5), 1218, doi:10.1029/2002JA009726.

Tanaka, M. (1996), Asymmetry and thermal effects due to parallel motion of electrons in collisionless magnetic reconnection, *Phys. Plasmas*, *3*, 4010.

Umeda, T., Y. Omura, H. Matsumoto, and H. Usui (2002), Formation of electrostatic solitary waves in space plasmas: Particle simulations with open boundary conditions, *J. Geophys. Res.*, *107*(A12), 1449, doi:10.1029/2001JA000286.

Zeiler, A., D. Biskamp, J. F. Drake, B. N. Rogers, M. A. Shay, and M. Scholer (2002), Three-dimensional particle simulations of collisionless magnetic reconnection, *J. Geophys. Res.*, *107*(A9), 1230, doi:10.1029/2001JA000287.

M. André, Swedish Institute for Space Physics, Uppsala Division, SE-75121, Uppsala, Sweden.

A. Balogh and E. Lucek, Space and Atmospheric Physics Group, Blackett Laboratory, Imperial College, London SW7 2BZ, UK.

C. A. Cattell, J. Dombeck, and J. R. Wygant, University of Minnesota–Twin Cities, School of Physics and Astronomy, 116 Church St. SE, Minneapolis, MN 55455, USA. (cattell@belka.space.umn.edu)

J. F. Drake and M. Swisdak, Institute for Research in Electronics and Applied Physics, University of Maryland at College Park, College Park, MD 20742, USA.

A. Fazakerley, Mullard Space Science Laboratory, University College London, Holmbury St. Mary, Dorking, Surrey RH5 6NT, UK.

M. L. Goldstein and W. Keith, NASA Goddard Space Flight Center, MC 692, Greenbelt, MD 20771, USA.